Semi-continuous propagation of influenza A virus and its defective interfering particles: analyzing the dynamic competition to select candidates for antiviral therapy

Lars Pelz[1,†], Daniel Rüdiger[1,†], Tanya Dogra[1,†], Fadi G. Alnaji[2], Yvonne Genzel[1], Christopher B. Brooke[2], Sascha Y. Kupke[1,*], Udo Reichl[1,3]

[1]Max Planck Institute for Dynamics of Complex Technical Systems, Bioprocess Engineering, Magdeburg, Germany

[2]University of Illinois at Urbana-Champaign, Department of Microbiology, Urbana, Illinois, USA

[3]Otto-von-Guericke-University Magdeburg, Bioprocess Engineering, Magdeburg, Germany

[†]These authors contributed equally to this work.

*** Correspondence:**

Sascha Y. Kupke

kupke@mpi-magdeburg.mpg.de

Keywords: Influenza A virus, defective interfering particles, antiviral, next-generation sequencing, continuous virus production

Abstract

Defective interfering particles (DIPs) of influenza A virus (IAV) are naturally occurring mutants that comprise an internal deletion in one of their eight viral RNA (vRNA) segments, rendering them propagation-incompetent. Upon co-infection with infectious standard virus (STV), DIPs interfere with STV replication through competitive inhibition. Thus, DIPs are proposed as potent

antivirals for treatment of the influenza disease. To select corresponding candidates, we studied *de novo* generation of DIPs and propagation competition between different defective interfering (DI) vRNAs in a STV co-infection scenario in cell culture. A small-scale two-stage cultivation system that allows long-term semi-continuous propagation of IAV and its DIPs was used. Strong periodic oscillations in virus titers were observed due to the dynamic interaction of DIPs and STVs. Using next-generation sequencing, we detected a predominant formation and accumulation of DI vRNAs on the polymerase-encoding segments. Short DI vRNAs accumulated to higher fractions than longer ones, indicating a replication advantage. Yet, a sweet spot of fragment length was observed. Some DI vRNAs showed breaking points in a specific part of their bundling signal (belonging to the packaging signal), suggesting its dispensability for DI vRNA propagation. Over a total cultivation time of 21 days, several individual DI vRNAs accumulated to high fractions, while others decreased. Using reverse genetics for IAV, purely clonal DIPs derived from highly replicating DI vRNAs were generated. We confirm that these DIPs exhibit a superior *in vitro* interfering efficacy than DIPs derived from lowly accumulated DI vRNAs and suggest promising candidates for efficacious antiviral treatment.

Importance

Defective interfering particles (DIPs) emerge naturally during viral infection and typically show an internal deletion in the viral genome. Thus, DIPs are propagation-incompetent. Previous research suggests DIPs as potent antiviral compounds for many different virus families due to their ability to interfere with virus replication by competitive inhibition. For instance, the administration of influenza A virus (IAV) DIPs resulted in a rescue of mice from an otherwise lethal IAV dose. Moreover, no apparent toxic effects were observed when only DIPs were administered to mice and ferrets. IAV DIPs show antiviral activity against many different IAV strains, including pandemic and highly pathogenic avian strains, and even against non-homologous viruses, like SARS-CoV-

2, by stimulation of innate immunity. Here, we used a cultivation/infection system, which exerted selection pressure toward accumulation of highly competitive IAV DIPs. These DIPs showed a superior interfering efficacy *in vitro*, and we suggest them for effective antiviral therapy.

1 Introduction

Yearly, on average 400,000 people globally die from an infection with seasonal influenza A virus (IAV) (1). Moreover, the potential emergence of pandemic strains is a major threat to public health (2). The most effective prevention of the influenza disease is vaccination with tri- or quadrivalent formulations, which provide protection against different influenza virus strains (3, 4). However, influenza vaccines have to be reformulated annually as a result of antigenic drifts (5). This is associated with a potential decrease in vaccine efficacy due to false predictions and a vaccine mismatch to circulating strains (6). Furthermore, antiviral drugs targeting the viral neuraminidase (oseltamivir, zanamivir) (7) or the viral endonuclease (baloxavir) (8) may also be used. Yet, circulating strains have already shown resistance against available antivirals (9-11). Therefore, the development of effective prophylactic and therapeutic treatment options is urgently needed.

One promising approach for antiviral therapy is the application of defective interfering particles (DIPs) (12-16). These naturally occurring viral mutants feature an internal deletion in one of their eight viral RNA (vRNA) segments, which renders them defective in virus replication. In addition, a new species of IAV DIPs that showed point mutations on segment (Seg) 7 vRNA was discovered recently (17). DIPs can only replicate in a co-infection with infectious standard virus (STV), which complements the respective defect in the replication of the DIPs. These viral mutants are believed to interfere by preferential and faster replication of the defective interfering (DI) vRNA in comparison to the full-length (FL) vRNA, thereby drawing away cellular and viral resources

74 required for STV growth (18-20). Furthermore, interference was shown at the packaging step, as
75 DI vRNAs can selectively outcompete FL vRNA packaging (21, 22). Notably, in mouse and ferret
76 models, the administration of DIPs resulted in a pronounced antiviral effect against IAV infection
77 (13, 14, 23-26). Furthermore, IAV DIPs also showed protection against heterologous interferon-
78 sensitive respiratory viruses (27, 28), including SARS-CoV-2 (29), by the ability to stimulate innate
79 immunity.

80 Recently, we established a two-stage bioreactor system for cell culture-based production of IAV
81 (for vaccine manufacturing) (30), and of a prototypic, well-characterized DIP ("DI244" (23, 24,
82 27)) (31). Here, uninfected cells (first bioreactor) were continuously fed to a second bioreactor that
83 contained virus-infected cells. However, in such a continuous culture, the co-infection of STVs and
84 DIPs typically result in periodic oscillations of virus titers due to their dynamic interactions.
85 Moreover, *de novo* generation and accumulation of numerous DI vRNAs was observed (30, 31).

86 In the present study, a simplified, semi-continuous setup was used to thoroughly investigate the
87 generation and growth competition between DIPs during 21 days of IAV infection. Assuming that
88 DIPs showing exceptional propagation also show high interfering efficacies, we anticipated
89 identification of potent candidates for antiviral therapy. For detection and quantification of the
90 different deletion junction on the IAV vRNA level, we used a recently published next-generation
91 sequencing (NGS) framework (32). We observed a small subset of highly accumulated DI vRNAs
92 after 21 days post infection (dpi), while other deletion junctions showed a pronounced decrease in
93 their fractions in the same timeframe. To generate corresponding purely clonal DIPs harboring the
94 promising candidate DI vRNAs, we used reverse genetics for IAV. Indeed, these DIPs displayed a
95 superior *in vitro* interfering efficacy compared to DIPs derived from lowly replicating DI vRNAs
96 indicating their potential for antiviral therapy.

2 Results

2.1 Semi-continuous production of IAV results in periodic oscillations of virus titers and strong accumulation of DIPs

In order to induce *de novo* generation and accumulation of DIPs, an IAV strain A/PR/8/34 of the subtype H1N1 (PR8, provided by Robert Koch Institute, Berlin, Germany) was propagated in a semi-continuous small-scale two-stage cultivation system (Fig. 1B). For infection, we used a seed virus that was depleted in DI vRNAs as shown by segment-specific reverse-transcription (RT-)PCR (Fig. 1A). Madin-Darby canine kidney (MDCK) cells growing in suspension culture (MDCK(sus)) were seeded into the cell seeding shake flask (CSS) and virus shake flasks (VS) at a viable cell concentration (VCC) of 0.6×10^6 cells/mL and grown in batch mode to about 3.0×10^6 cells/mL (-1.6 dpi) (Supplementary Fig. 1). Subsequently, for both shake flasks, a calculated volume of cell suspension was discarded and fresh medium was added at regular time intervals (both shake flasks not yet connected in series). This resulted in a residence time (RT) of 38.3 h for both vessels. Note that preliminary studies showed a steady state in the VCC for this RT (data not shown). Once the steady state was reached (Supplementary Fig. 1), cells in the VS were infected with PR8 at an MOI of 0.1. At 0.5 dpi, both vessels were connected in series and, from thereon, cells transferred semi-continuously from the CSS to the VS (V_2). In addition, fresh medium was added to both shake flasks (V_1 or V_3) and virus harvest was taken (V_4). The RT chosen was 38.3 h and 22.0 h for CSS and VS, respectively, as this previously resulted in pronounced titer fluctuations and strong accumulation of DIPs (31). Over the production time of 21 dpi, the steady state in the CSS was kept with an average VCC of 2.6×10^6 cells/mL (SD of $\pm 0.2 \times 10^6$ cells/mL) (Supplementary Fig. 1).

Strong periodic oscillations in the infectious virus titers (quantified by $TCID_{50}$ assay) and in the extracellular vRNA level of Seg 5 (quantified by real-time RT-qPCR) were observed in the VS (Fig. 1C). The extracellular vRNA level of Seg 5 was taken as a measure of the total virus concentration. DI vRNAs are mostly located on polymerase-encoding segments (20, 33-36), so the occurrence of DIPs should not affect the detection of Seg 5 vRNA. Shortly after infection at 0.5 dpi, a maximum infectious virus titer of 5.6×10^8 $TCID_{50}$/mL was reached. Here, high concentrations of STV (complying with a high MOI) increased the chance for co-infections with DIPs. Thus, a strong DIP propagation likely occurred early in cultivation, impeding STV propagation. Therefore, infectious virus titers decreased from 0.5 dpi onwards. Eventually, the declining infectious virus titers led to fewer co-infections. Thus, DIP replication decreased, and the total virus particle concentration dropped as well. Additionally, DIPs were out-diluted because of the semi-continuous feeding strategy. Then, at a low infectious virus concentration (complying with a low MOI condition, ~4.0 dpi), the chance of DIP co-infections was supposedly significantly reduced. In these conditions, STVs could accumulate again as indicated by increasing virus titers toward 5 dpi. In the following, further periodic oscillations in virus titers occurred based on the DIP/STV interaction described above.

The dynamics in virus titers were well in agreement with results of the segment-specific RT-PCR (indicating FL and DI vRNAs) (Fig. 1D). A rapid accumulation of DI vRNAs occurred already at 0.5 dpi. Furthermore, the FL vRNA signal gradually dropped between 1 dpi and 2.5 dpi, suggesting the preferential production of DI vRNAs. Subsequently, DI vRNA replication decreased and DI vRNAs were washed out, as indicated by weaker band intensities of DI vRNAs (e.g. at 8.5 dpi). Next, in agreement with the increase of infectious viral titers (STVs), FL vRNA bands were visible again (e.g. at 9 dpi). Moreover, agarose gels indicated the presence of DI vRNA bands at the end of cultivation that may have been already present in the seed virus, suggesting that some DI vRNAs

were preserved. In addition, weak DI vRNA bands as well as undefined, blurred bands emerged during the course of IAV replication, suggesting the formation and accumulation of *de novo* generated DI vRNAs.

In summary, the semi-continuous production of IAV using a seed virus depleted in DI vRNAs led to the accumulation of DIPs. Thus, strong periodic oscillations in the total concentration of virions and infectious virus titers were observed due to the dynamic interaction of STVs and DIPs. Moreover, in the course of production, DIPs were exposed to high and low MOI conditions that have likely resulted in alternating selection pressures, suitable for potential selection toward accumulation of highly interfering DIPs.

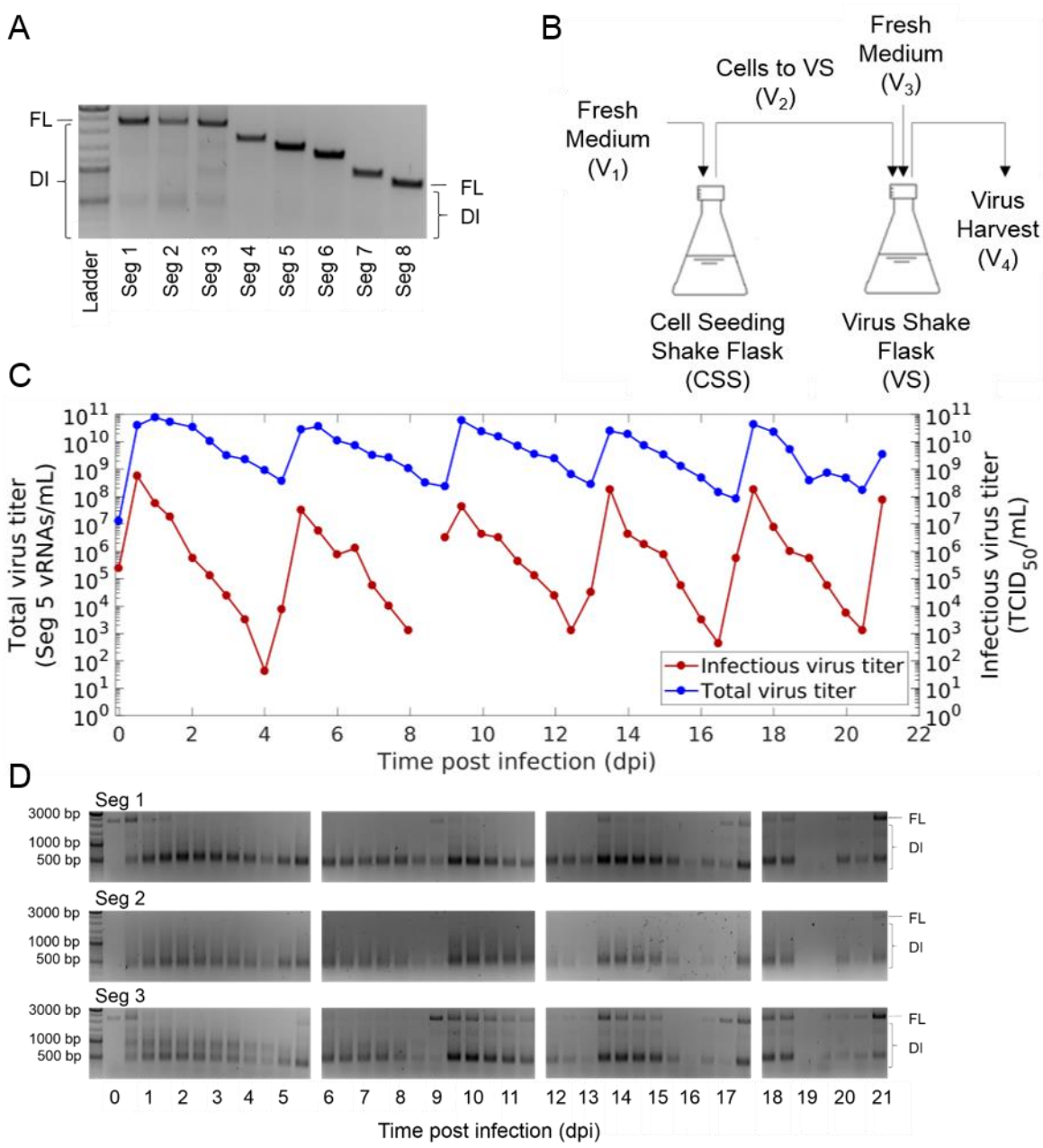

Figure 1: Semi-continuous propagation of influenza A virus and DIPs. (A) PR8 seed virus depleted in DI vRNAs was used for infection. Results of segment-specific RT-PCR for Seg 1 to 8 followed by agarose gel electrophoresis are shown. Signals corresponding to FL and DI vRNAs are indicated. Upper, middle and lower thick bands of the DNA ladder indicate 3000, 1000 and 500 bp, respectively. (B) Experimental setup of the small-scale two-stage cultivation system in shake flasks (scheme adapted from F. Tapia et al. (37)). MDCK(sus) cells were grown in the CSS and VS. After an initial batch and semi-continuous phase (CSS and VS not coupled), the cells in the VS were infected with the seed virus (A) at an MOI of 0.1. The semi-continuous production mode was initiated 0.5 dpi, where cells were transferred from the CSS into the VS (V_2) at regular time intervals, while fresh medium was added (V_1 or V_3) and virus harvest was taken for monitoring (V_4). (C) Periodic oscillations of total and infectious virus titers during the production. vRNA level of Seg 5 (indicating total virus particle concentration) was quantified by real-time RT-qPCR

and infectious virus titer by $TCID_{50}$ assay. D) Accumulation of DI vRNAs over the semi-continuous production time of 21 days. Results of the segment-specific RT-PCR are shown for Seg 1, 2, and 3. Signals corresponding to FL and DI vRNAs are indicated. Illustration includes results of one experiment.

2.2 Next-generation sequencing results indicate predominant *de novo* formation and accumulation of deletion junctions on polymerase-encoding segments

Segment-specific RT-PCR does not enable the detection and quantification of individual deletion junctions. Therefore, to study the diversity of DI vRNAs generated during semi-continuous IAV propagation, samples were subjected to Illumina-based NGS and processed by a bioinformatics pipeline (32). Doing so, sequences of vRNAs from the produced progeny virions were obtained. Reads comprising a deletion junction (DI vRNA reads) do not align to the corresponding reference genome. These NGS reads were processed by the ViReMa algorithm to identify the position of individual deletion junctions (38).

The highest variation (i.e., number of different deletion junction) was found on the polymerase-encoding segments 1–3, which encode for the polymerase basic protein 2 (PB2) and 1 (PB1), and polymerase acidic protein (PA), respectively (Fig. 2A). Fig. 2B shows the fraction of all deletion junctions located on a genome segment over time. Here, polymerase-encoding segments showed the highest fraction. In contrast, deletion junctions of non-polymerase-encoding segments showed a significantly lower fraction, which increased slightly toward the end of cultivation but always remained below 2%. As non-polymerase segment deletion junctions occurred only in negligible numbers, they were not considered any further in subsequent analyses.

Next, we investigated the *de novo* formation of DI vRNAs over the course of the cultivation. Fig. 2C shows, at specific time intervals, the number of *de novo* generated deletion junctions. *De novo* formation occurred mainly on the polymerase-encoding segments. Interestingly, most *de novo*

formations occurred within the first 1.5 dpi. In addition, a considerable number of *de novo* DI vRNAs was detected between 3.5–5.5 dpi. However, *de novo* formation was significantly lower at later time points. Moreover, an increase in the number of new deletions was highly correlated with an increase in the total virus particle concentration (indicated by the vRNA level of Seg 5) (Fig. 2C). This is consistent with a fast STV replication, and thus, likely with a higher occurrence of the *de novo* formation of DI vRNAs due to the error-prone nature in the replication of the IAV RNA-dependent RNA polymerase.

In sum, our results show that DI vRNAs are predominantly *de novo* formed and accumulated on the polymerase-encoding segments during semi-continuous IAV infection.

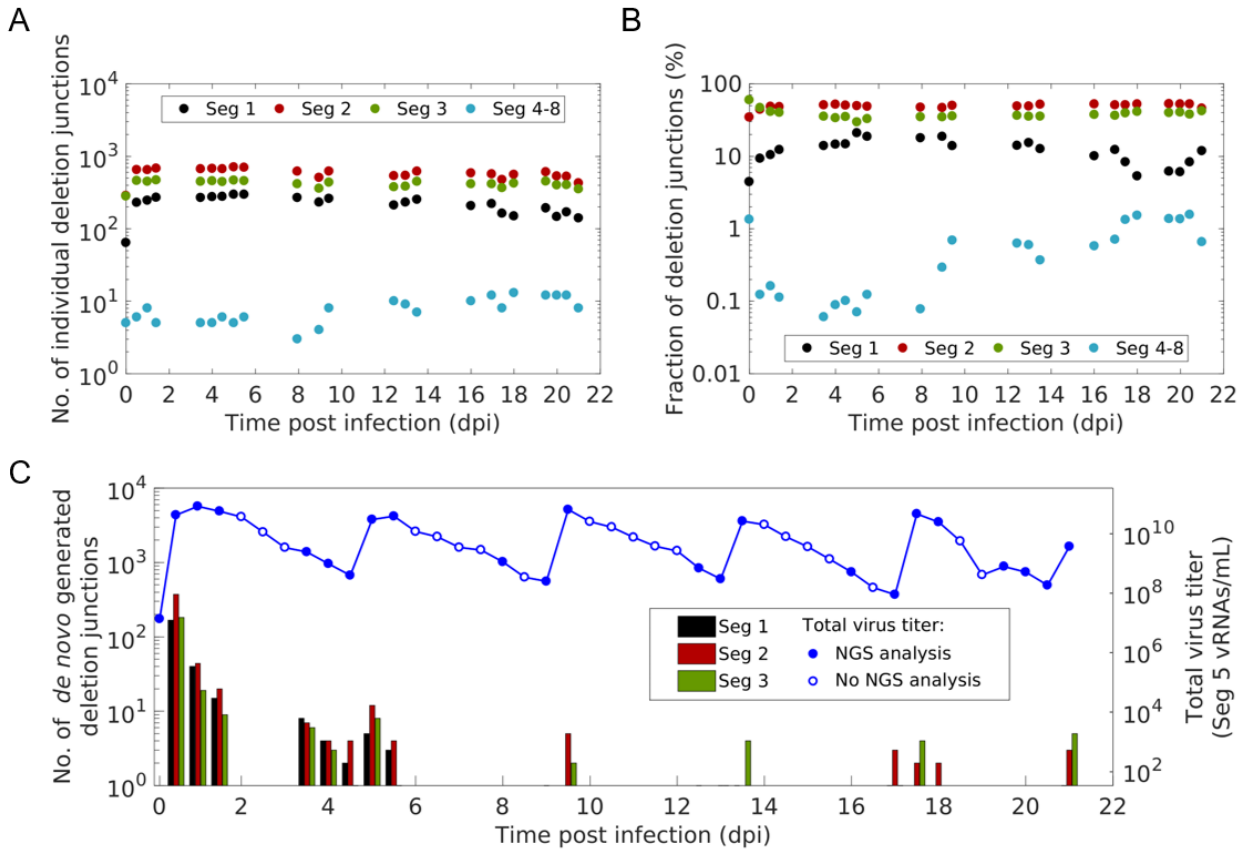

Figure 2: Diversity, distribution and *de novo* generation of deletion junctions during semi-continuous propagation of IAV. Deletion junctions were identified by Illumina-based NGS and subsequent analysis via the ViReMa algorithm (32). (A) Number of different deletion junctions located on the respective genome segment(s). (B)

Fraction of all deletion junctions located on the respective genome segment(s). This fraction describes the ratio of the total number of detected deletion junctions for one segment to the total number of deletion junctions on all genome segments**.** (C) *De novo* formation of deletion junctions. vRNA level of Seg 5 (indicating total virus particle concentration, as shown in Fig. 1C) was quantified by real-time RT-qPCR. Samples not analyzed by NGS are indicated by blank dots. Illustration includes results of one experiment.

2.3 Short DI vRNAs tend to accumulate to higher fractions than longer ones; yet, intermediate length sweet spots were observed as well

It was reported that DI vRNAs accumulation surpasses that of FL vRNAs due to their shorter length resulting in a supposedly faster replication (12, 20). Therefore, we speculated that shorter DI vRNAs may also accumulate to higher abundances than longer DI vRNAs. Fig. 3 shows the fraction of all individual deletion junctions and their corresponding DI vRNA length. Indeed, a bias toward accumulation of shorter DI vRNAs was observed with short DI vRNAs showing overall higher fractions than longer ones during semi-continuous IAV production (Fig. 3). However, highest fractions were not found for the shortest DI vRNAs. It rather appeared that highest fractions were found at a length sweet spot. To visualize this sweet spot, we fitted a normal distribution function to the DI vRNA length (Supplementary Fig. 2), and plotted the resulting mean as a dashed vertical line (Fig. 3). Over the whole cultivation, the mean DI vRNA length ranged between 366–414 nt, 425–534 nt, and 434–557 nt for Seg 1, 2, and 3, respectively.

Moreover, a few larger DI vRNAs (comprising a sequence length of up to 1000 nt) accumulated to high fractions, suggesting that the sequence and the position of the deletion junction may be another factor to consider for replication of a DIP (Fig. 3). Note that Fig. 3 only shows DI vRNAs up to 1000 nt in length, although we also detected very long DI vRNAs (>2000 nt) (Supplementary Fig. 3). These DI vRNAs with very short deletions may either not result in a defective vRNA, comprise two deletions or represent technical artifacts. Due to their unknown origin and function

and a lack of description in the literature, defective vRNAs larger than 85 % of its respective FL length were excluded from analysis in this work (shown in Supplementary Fig. 3).

Taken together, shorter DI vRNAs showed an overall stronger accumulation compared to longer DI vRNAs. However, highest fractions were found at a sweet spot, indicative for an optimal length for efficient DI vRNA replication and spreading.

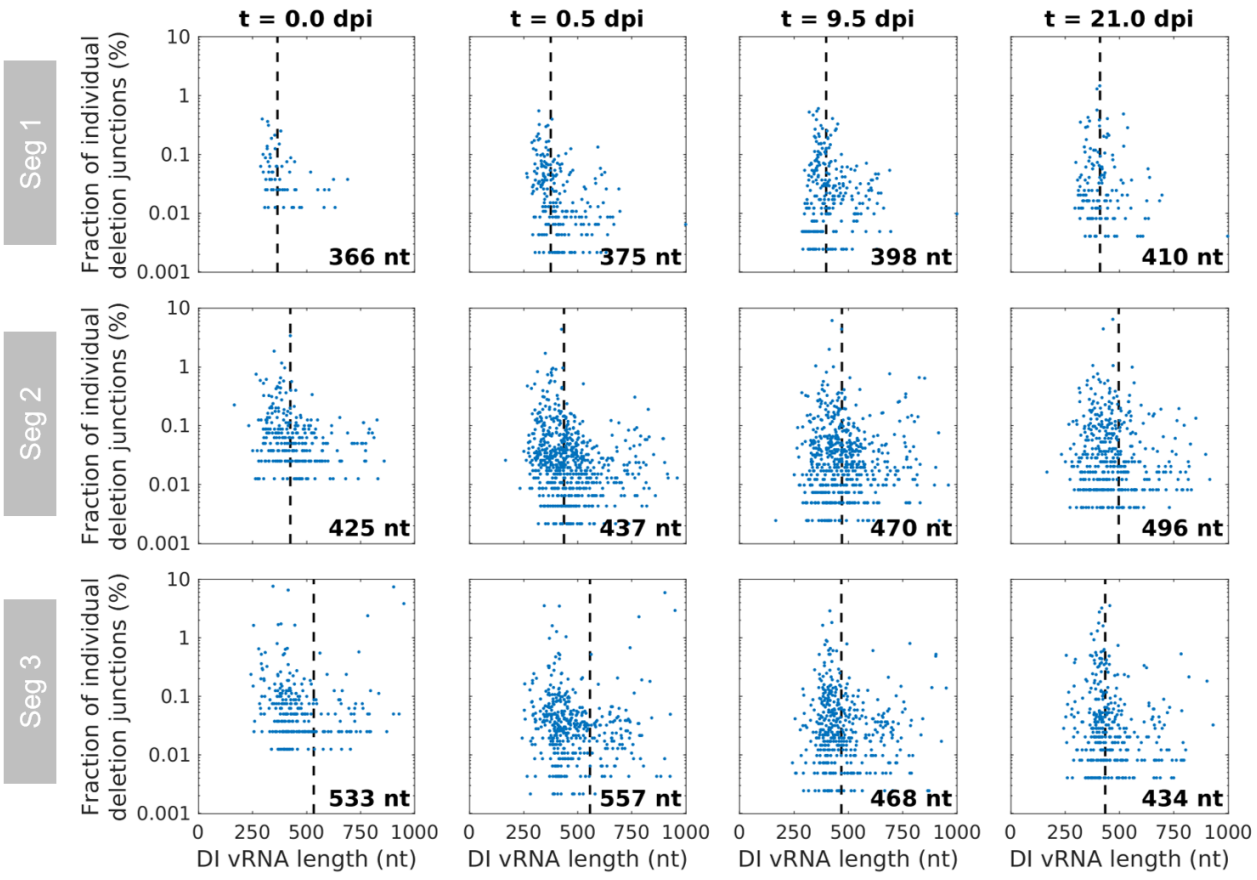

Figure 3: Dependency of the length of DI vRNAs on their accumulation during semi-continuous propagation of IAV. Deletion junctions were identified by Illumina-based NGS and subsequently analyzed via the ViReMa algorithm (32). Fractions of individual deletion junctions were calculated based on the ratio of the number of NGS reads of one individual deletion junction to the number of NGS reads of all deletion junctions located on all eight segments. Means of DI vRNA length (calculated by fitting a normal distribution function) are indicated by dashed vertical lines and corresponding lengths are shown. Representative time points are illustrated. Illustration includes results of one experiment.

2.4 The incorporation signal but not the entire bundling signal appears to be required for propagation of DIPs

We next examined the position of the breaking points of DI vRNAs. Fig. 4 illustrates the position of individual deletion junctions, as indicated by the number of retained nucleotides prior (DI vRNA 3´ length) and after (DI vRNA 5´ length) the deletion junction site. In the course of the semi-continuous cultivation, breaking points were mostly located in proximity to both ends of vRNA (Fig. 4). This finding is in line with our observation of the predominant accumulation of short DI vRNAs (Fig. 3.). We also observed highly abundant medium-sized DI vRNAs on Seg 3 in the seed virus (0.0 dpi). Yet, the fraction of DI vRNAs carrying these deletions decreased, or even disappeared toward the end of cultivation (Fig. 3). Again, this indicates that shorter DI vRNAs replicate faster and may outcompete longer ones. Additionally, the 3´ length of the DI vRNA did largely not correlate with the 5´ length, suggesting that deletion junctions are not preferably symmetrical.

While the lengths of the 3´ and 5´ ends ranged from below 100 nt to over 500 nt, specific minimum lengths were retained in the DI vRNAs (Fig. 4). We then asked whether the complete packaging signal (situated at the terminal ends of vRNA), which is important for organized packaging into progeny virions (39), was unaffected by deletions. A small percentage of breaking points was located in the packaging signal (on Seg 1 and 2); yet, the majority of the deletion junction sites were located outside of it, which is in line with the observation of a sweet spot in DI vRNA length (Fig. 3). For a more thorough investigation of deletion junctions in the packaging signal, we highlighted the positions of the incorporation signal (non-coding region (NCR), including the promoter region) and the bundling signal (terminal ends of coding region) (40). The incorporation signal was reported to lead the packaging of the vRNA in which the signal is found. The second

261 part of the packaging signal is the bundling signal, which confers the selective packaging of all the
262 eight different segments together (40). We checked which part of the sequence at both ends were
263 retained to infer a minimum sequence length for functional replication and packaging of the
264 truncated vRNAs, assuming that only propagation-competent DI vRNAs can be detected. No
265 deletion junctions in the incorporation signal for the polymerase-encoding segments as well as for
266 Seg 4–8 were identified (Fig. 4, Supplementary Fig. 4, respectively). Therefore, we suggest that
267 the preservation of the entire incorporation signal is crucial for the propagation of DIPs

268 Interestingly, deletion junctions in the bundling signal (on Seg 1 and 2) could be detected,
269 indicating that the entire bundling signal of these segments is most likely not required for
270 propagation of DIPs. In particular, clusters of DI vRNA breaking points in the bundling signal were
271 stable and present over the complete course of the semi-continuous cultivation. In contrast, Seg 3
272 did not show any breaking points in both signals. We found a minimum sequence length of 84 nt
273 (3´ end) and 100 nt (5´ end), 25 nt and 95 nt, and 82 nt and 95 nt for Seg 1, 2, and 3, respectively.
274 Supplementary Fig. 4 shows the position of deletion junction sites in Seg 4–8. Notably, although
275 only very few individual deletion junctions were detected, breaking points were found in the
276 bundling signal on Seg 6 (3´ end), Seg 7 (both ends), and Seg 8 (5´ end) as well.

277 In summary, our results indicate that the complete incorporation signal is crucial for propagation
278 of DIPs. Yet, only a part of the bundling signal in Seg 1 and 2 seem to be required for DIP
279 spreading.

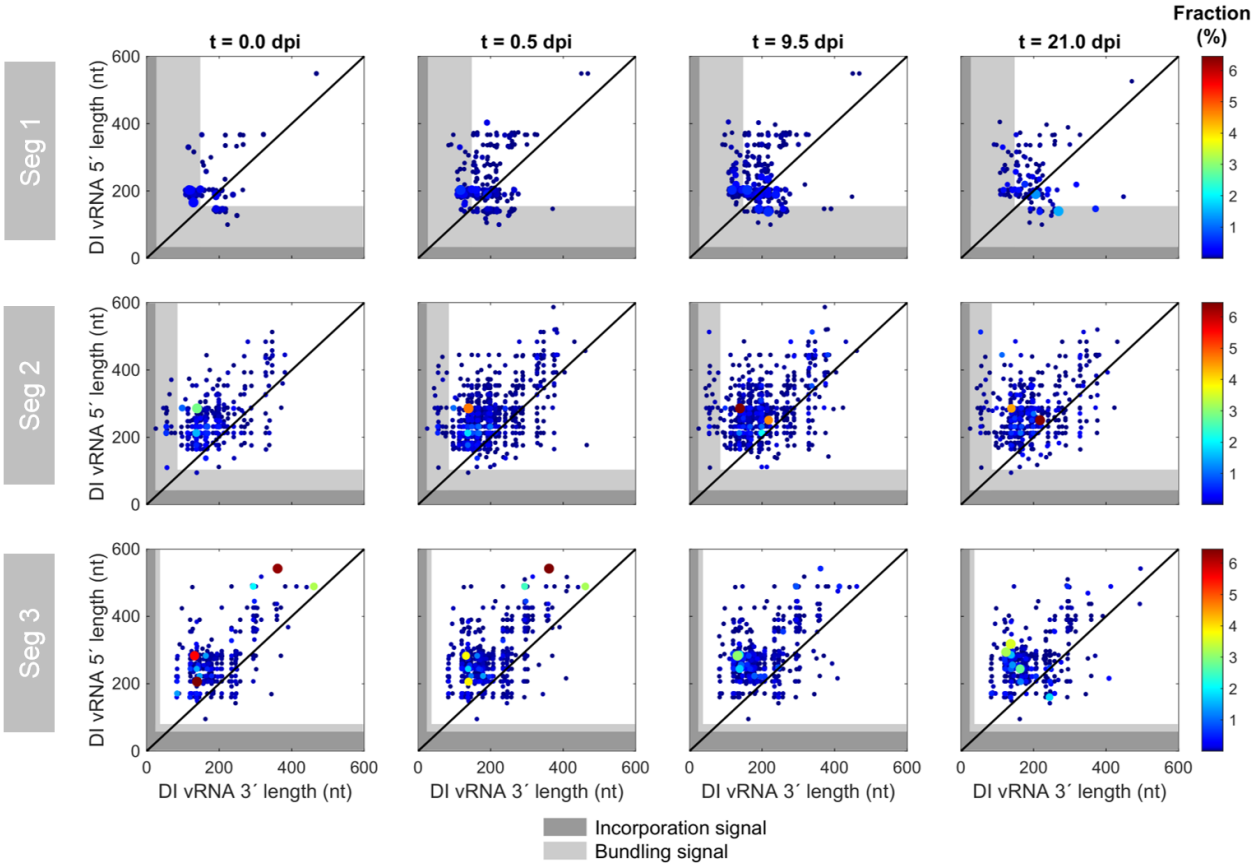

Figure 4: Deletion junction sites of DI vRNAs during semi-continuous propagation of IAV. Deletion junctions were identified by Illumina-based NGS and subsequently analyzed via the ViReMa algorithm (32). DI vRNA 3´ and 5' length indicate the number of retained nucleotides prior and after the deletion junction, respectively, at the corresponding vRNA ends. The packaging signal is indicated as grey areas, which is divided into the incorporation signal (dark grey area) and bundling signal (light grey area). Representative time points are illustrated. The color code from red to blue shown on the right denotes the fraction of individual deletion junction, which was calculated based on the ratio of the number of NGS reads of one individual deletion junction to the number of NGS reads of all deletion junctions located on all eight segments. Additionally, the circle radii increase with higher fractions. The diagonal black line indicates an equal DI vRNA 3´ and 5´length. Illustration includes results of one experiment.

2.5 Dynamic competition in propagation between DI vRNAs leads to selection toward accumulation of highly interfering DIPs

In order to elucidate whether the various DI vRNAs show differences in their propagation, we next studied the composition of deletion junctions over cultivation time. More specifically, we

295 determined the fraction of each individual deletion junction over time. Fig. 5A shows these
296 fractions and highlights the top five deletion junctions that showed the highest gain or largest loss
297 in their fraction from the seed virus (0 dpi) to the end of cultivation (21 dpi). Likewise, the top five
298 gains of *de novo* formed DI vRNAs are indicated. Interestingly, differences between gains and
299 losses were very pronounced, with a decreasing fraction of the top five losses, while the top five
300 gains (including *de novo*) showed a strong accumulation. These trends were most prominent for
301 Seg 3. Of note is also one deletion junction on Seg 2 that was present at a very high fraction in the
302 seed virus and throughout the whole cultivation. Furthermore, pronounced shifts in the composition
303 of deletion junctions were found for 9–9.5 and 17–17.5 dpi, at best visible for Seg 3. The
304 occurrence of DI vRNAs that accumulate faster and achieve higher fractions than other DI vRNAs
305 suggests that there was a dynamic competition in the propagation between individual DI vRNAs.

306 Moreover, we examined whether top gains (including *de novo*) and losses show differences in the
307 deletion junction position (Fig. 5B). To obtain a better overview, we expanded the number of the
308 top candidates in each category to 15. However, it appeared that no clear differences between the
309 groups were present. For both gains and losses, few deletion junction sites were located in the
310 bundling signal for Seg 1 and 2 (although most were found outside (Fig. 5B)), but none for Seg 3.
311 Therefore, even for competitive DIPs (which require an efficient packaging process), we found a
312 shorter packaging signal compared to the FL vRNA on Seg 1 (both ends) and on Seg 2 (3´ end).
313 Please also note a few DI vRNAs (belonging to the top 15 losses) on Seg 3 showing a medium-
314 sized DI vRNA length (~900 nt) (Fig. 5B, upper right corner), which is in line with our observation
315 that long DI vRNAs accumulate to low fractions (Fig. 3). Yet, we also found two top 15 gains (*de*
316 *novo*) on Seg 2 with a very long DI vRNA (1905 nt and 1628 nt) (Supplementary Fig. 5). This
317 finding might suggest that not only the sequence length but also the breaking point position and
318 probably further unknown regulatory effects are crucial for the efficient propagation of DI vRNAs.

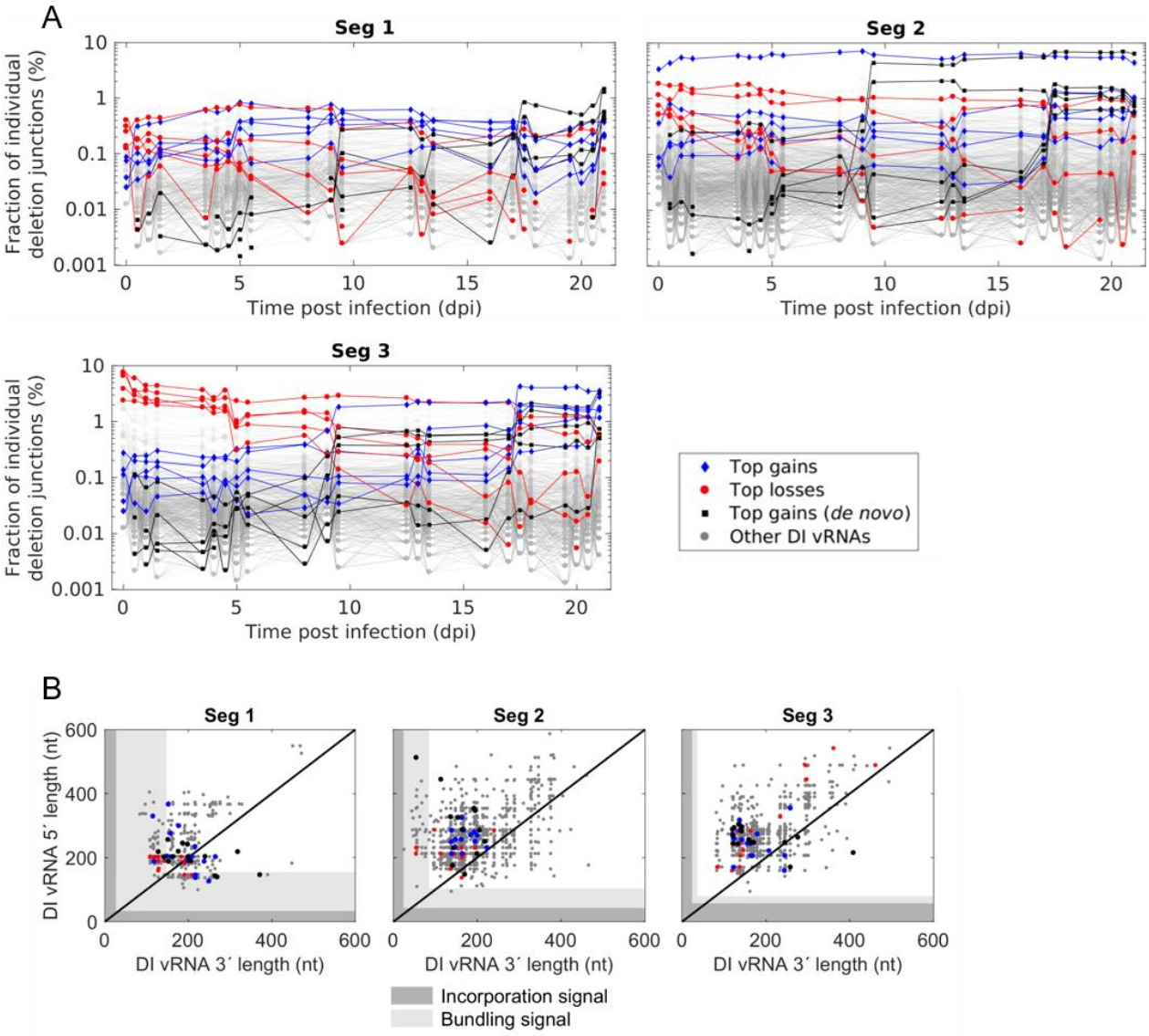

Figure 5: Propagation of DI vRNAs showing highest gains or losses in their fractions during semi-continuous propagation of IAV. Deletion junctions were identified by Illumina-based NGS and subsequently analyzed via the ViReMa algorithm (32). Fractions of individual deletion junctions were calculated based on the ratio of the number of NGS reads of one individual deletion junction to the number of NGS reads of all deletion junctions located on all eight segments. (A) Fraction of individual DI vRNAs belonging to the group of top five gains, losses, and gains (*de novo*) of the fraction over cultivation time. Top gains (*de novo*) indicate newly formed deletion junctions with the highest fraction at the end of cultivation. (B) Deletion junction position of the top 15 gains, losses, and gains (*de novo*). DI vRNA 3´ and 5' length indicate the number of retained nucleotides prior and after the deletion junction, respectively, at the corresponding vRNA ends. The packaging signal is indicated as grey areas, which is divided into the incorporation signal (dark grey area) and bundling signal (light grey area). Illustration includes results of one experiment.

In order to test the hypothesis, that fast-propagating DI vRNAs show a higher interfering efficacy than slow-propagating ones, we reconstituted the corresponding DIPs and tested them in an *in vitro* interference assay. More specifically, we rescued purely clonal DIPs (in the absence of STV) harboring either the top gain, top loss, or top gain (*de novo*) DI vRNA of Seg 1 (Supplementary Table 5) using a modified reverse genetics system for IAV DIPs (25, 41). Next, we propagated these selected DIPs in genetically engineered MDCK-PB2(sus) cells, expressing PB2 (Supplementary Fig. 6), to allow multiplication of these DIPs (harboring a deletion in Seg 1) without STV through complementation. Almost complete absence of contamination with other DI vRNAs was confirmed by results of segment-specific RT-PCR (Supplementary Fig. 7).

In the *in vitro* interference assay (Fig. 6), adherent MDCK cells (MDCK(adh) cells were infected with STV at an MOI of 0.01 and co-infected with the different DIPs to evaluate the inhibition of STV replication compared to infection with STV alone (NC). Here, the DIP input for the interference assay was normalized through dilution based on the concentration of DIPs to ensure a direct comparison between the DIPs (Supplementary Table 7). In addition, we compared the interfering efficacy to a prototypic, well-characterized DIP named DI244 (23-25, 27). Indeed, the DIPs derived from the top gains (including *de novo*) showed the highest interfering efficacy. The top gain (*de novo*) DIP reduced the infectious virus release by more than five orders of magnitudes, the top gain by five logs, while top loss and DI244 showed a reduction of only four orders of magnitudes. Reduction of the total virus particle release, indicated by the HA titer, showed a similar trend (Fig. 6B).

In summary, our results indicate that the semi-continuous propagation of IAV led to a dynamic competition in propagation between different DI vRNAs. We demonstrate that DI vRNAs showing the highest increase in the fraction over the cultivation period result in the formation of DIPs that

354 show a superior interfering efficacy compared to DIPs containing slowly propagating DI vRNAs.
355 These DIPs are, thus, promising candidates for antiviral therapy.

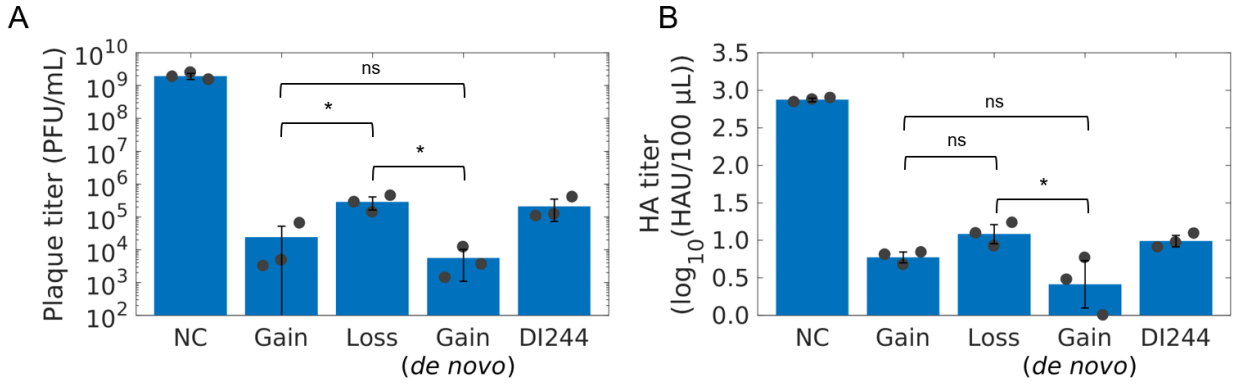

356

357 **Figure 6: Interfering efficacy of DIPs derived from DI vRNAs showing highest gain, loss or gain (*de novo*) in**
358 **their fraction during semi-continuous propagation of IAV.** Purely clonal DIPs containing a deletion in Seg 1
359 (derived from DI vRNAs showing top gains and top loss) were generated using a modified reverse genetics
360 methodology for reconstitution of purely clonal IAV DIPs (41). Next, DIPs were multiplied in genetically engineered
361 MDCK-PB2(sus) cells (expressing PB2) in shake flask at a multiplicity of DIP (MODIP) E-2 (Supplementary Fig. 6).
362 (A and B) Interference assay. MDCK(adh) cells were infected with STV only at an MOI of 0.01 (NC) or co-infected
363 with the corresponding DIP resulting in a DIP/STV ratio of 3224 (number of DIPs: 4.25×10^8 virions, number of
364 STVs: 1.32×10^5 virions, derived from the HA titer, Supplementary Table 7). For comparison, DI244, a prototypic,
365 well-characterized DIP (23-25, 27), was used. (A) Infectious virus release, quantified by plaque assay. (B) Total virus
366 particle release, measured by HA assay. Illustration includes results of three independent experiments (n = 3). Error
367 bars indicates standard deviation. One-way ANOVA followed by Tukey´s multiple comparison test (* $p < 0.05$; ns
368 $p > 0.05$, not significant) was used to determine significance.

369
370 ## 3 Discussion

371 IAV DIPs have been proposed as an effective antiviral agent for the influenza disease. In this study,
372 we investigated the *de novo* generation and the competition in the growth between a diversity of
373 DIPs during long-term semi-continuous IAV infection in order to identify strong candidates for
374 antiviral therapy. In general, DIPs and STVs are in a competition for cellular and viral resources
375 in a co-infection scenario (19, 42). Due to replication advantage of DIPs, suppression of and
376 interference with STV replication occurs (18-20). Moreover, it was shown that DIPs interfere with

377 STV propagation at the packaging step, as preferential incorporation of DI vRNAs over FL vRNAs
378 was observed (21, 22). We, thus, hypothesized that DI vRNAs showing the strongest accumulation
379 during long-term co-infection possess the highest interference efficacy with STV replication. In
380 our experiments, a small subset of individual DI vRNAs was observed that showed a pronounced
381 accumulation while the fractions of some other DI vRNAs strongly decreased (Fig. 5A). Next,
382 DIPs harboring the most competitive DI vRNAs on Seg 1 were generated and we show that these
383 DIPs exhibit a higher interfering efficacy than slowly propagating ones (Fig. 6). Strikingly, the
384 interfering efficacy was also higher in comparison to DI244, a prototypic and well-characterized
385 DIP (23-25), suggesting a huge potential of these candidates for antiviral treatment.

386 Our data show that the most competitive DI vRNAs are derived from the polymerase-encoding
387 segments. Further, we found the highest variation, accumulation and *de novo* formation of DI
388 vRNAs on these segments (Fig. 2A, Fig. 2B, Fig. 2C, respectively). This confirms previous
389 studies, which showed that DI vRNAs are predominantly found on Seg 1, 2, and 3 (20, 33-36). In
390 agreement with this, a bias toward the emergence of DI vRNAs on the polymerase-encoding
391 segments was observed during production of IAV over 17 d in a fully-continuous two-stage
392 bioreactor system (30). Mathematical modeling of the intracellular replication during STV and DIP
393 co-infection also suggested that DI vRNAs located on the polymerase-encoding segments are more
394 competitive than DI vRNAs on other segments (18). In particular, they even yielded high progeny
395 numbers in less advantageous infections scenarios, i.e., when STV co-infection was delayed by
396 several hours. Accordingly, in *in vivo* studies, DI244 containing a deletion on Seg 1, or DI vRNAs
397 carrying deletion in Seg 1, 2 or 3 showed a pronounced antiviral effect upon administration against
398 IAV replication in mice and in ferrets (14, 23-25)

Our results show that short DI vRNAs tended to accumulate to higher fractions than longer DI vRNAs (Fig. 3). In general, it is believed that the shorter length of DI vRNAs (in comparison to FL vRNAs) leads to a replication advantage (18-20), which supports our findings. However, our observation of a length sweet spot also indicates an optimal length for DI vRNA replication and spreading (Fig. 3). In agreement with this, the highly potent DI244 (395 nt) shows a similar DI vRNA length (Fig. 3) (23-25, 27). Other studies reported a similar mean DI vRNA length of 400–500 nt for Seg 1, 2, and 3 (12, 34). For DIPs originating from clinical isolates, a similar mean DI vRNA length of 377 nt (Seg 1), 390 nt (Seg 2), 490 nt (Seg 3) was found (36). Another investigation confirmed the finding of a replication advantage toward shorter vRNAs, but additionally suggested that the sequence (UTRs and coding region) may also have an influence on vRNA competition (42). This is consistent with a previous work proposing that not only the length, but also the sequence (or the deletion junction position) may drive the replication advantage of DI vRNAs (20). This may explain our observation of few larger DI vRNAs up to 1000 nt, which accumulated to high fractions (Fig. 3). In addition, two very long DI vRNAs (1905 nt and 1628 nt) were included in the top 15 gains (*de novo*) DI vRNAs (Supplementary Fig. 5). In further agreement, the *in vivo* interfering efficacy of three clonal DIPs containing DI vRNAs with a similar length (but diverse deletion junctions), differed significantly from each other (24). We found no clear patterns between the deletion junction positions of top gains (including *de novo*) and losses (Fig. 5B). These results may support the hypothesis that not only the DI vRNA length, but also the deletion junction site and further unknown regulatory effects are decisive factors for a competitive DI vRNAs.

Packaging of progeny virions of IAV is a complex process. The leading packaging model postulates a selective packaging of the eight different vRNA genome segments (43, 44). Decisive

for correct and efficient packaging is a special vRNA sequence (packaging signal), which was discovered using reverse genetics approaches (39). As DIPs comprise a truncated segment, this packaging signal might equally be affected. However, it was suggested that this packaging signal in the shortened segment typically remains intact (12, 43). The packaging signal is divided into two parts, the incorporation signal (NCR, including promoter region) and the bundling signal (located at the terminal ends of the coding region). Our results show that the incorporation signal is crucial for DIP propagation as it was unaffected by deletions (Fig. 4). However, several deletion junction sites were located in the bundling signal (Fig. 4, Fig. 5B, Supplementary Fig. 4). Therefore, we suggest that DIPs require only a part of the bundling signal for efficient replication and spreading. This finding does not agree with a previous study, which implied that the entire packaging signal of is crucial for DI vRNA stability (45) and for high interference (46).

Previous works showed that DI vRNAs interfere with FL vRNAs at the packaging process, by selectively suppressing the packaging either of the parent segment (21, 22) or the FL vRNA of another genome segment (47). However, one recent study showed the opposite, in which DI vRNA were packaged less frequently than FL vRNA (previously posted on a preprint server (48)). Furthermore, differences in the packaging rates were found between individual DI vRNAs (21, 46). Thus, the highly abundant DI vRNAs found in the present study may have an advantage in the entire propagation process over others, including both replication and packaging. Yet, further in-depth studies are required to better characterize the interference of DI vRNAs at the virus assembly step.

Taken together, we show that DIPs containing DI vRNAs with a superior propagation rate also show a superior capacity to interfere with STV replication. These DIPs are very interesting candidates for antiviral treatment. The highly competitive DI vRNAs are predominantly located on

the polymerase-encoding segments, display an optimal DI vRNA length, and conserve the incorporation signal, but do not require the entire bundling signal. In addition, yet unidentified sequence motifs certainly also play an additional role during DI vRNA propagation. Due to the complex features of highly competitive DIPs, the best candidates for antiviral therapy are probably challenging to design *in silico*. Thus, evolution studies are a more convenient screening tool as shown for DIPs of other virus families (49-51).

4 Materials and Methods

4.1 Cells and viruses

MDCK(adh) cells (ECACC, No. 84121903) were adapted in previous works to grow in suspension culture (52), and then in chemically defined Xeno™ medium (53), in this work referred to as MDCK(sus) cells. Further, this cell line was engineered to stably express the PB2 for the production of purely clonal DIPs harboring a DI vRNA in Seg 1 (25, 41) and is denoted as MDCK-PB2(sus). Cultivation of both cell lines was conducted in shake flasks at a working volume of 50 mL (125 mL baffled Erlenmeyer Flask, Thermo Fisher Scientific, 4116-0125) using an orbital shaker (Multitron Pro, Infors HT; 50 mm shaking orbit) at 185 rpm and 37°C in a 5% CO_2 environment. The medium was supplemented with 8 mM glutamine. For MDCK-PB2(sus) cells, puromycin (Thermo Fisher Scientific, #A1113803) was added at a final concentration of 0.5 µg/mL. Quantification of VCC, viability and diameter were performed using a cell counter (Vi-Cell™ XR, Beckman coulter, #731050). MDCK(adh) cells were maintained in Glasgow minimum essential medium (GMEM, Thermo Fisher Scientific, #221000093) supplemented with 10% fetal bovine serum and 1% peptone at 37°C and 5% CO_2. The corresponding adherent MDCK cell line that stably express PB2 (MDCK-PB2(adh)) (41) was maintained in the presence of 1.5 µg/mL

puromycin. Adherent PB2-expressing HEK-293T (HEK-293T-PB2) cells (41) were maintained in Dulbecco's Modified Eagle Medium (DMEM, Gibco, #41966029) supplemented with 10% fetal bovine serum, 1% penicillin streptomycin (10,000 units/mL penicillin and 10,000 µg/mL streptomycin, Gibco, #15140122) and 1 µg/mL puromycin at 37°C and 5% CO2.

For virus infection during semi-continuous cultivation, PR8 (provided by Robert Koch Institute, Berlin, Germany) was used (53). The strain was adapted to MDCK(sus) cells and depletion of DI vRNAs was carried out over five passages at a very low MOI of 10^{-5}. For the interference assay in MDCK(adh) cells, the same PR8 strain, but adapted to adherent MDCK cells was used. In addition, we generated candidate DIPs containing a deletion in Seg 1 using reverse genetics as described in chapter 4.6.

4.2 Small-scale two-stage cultivation system for semi-continuous STV/DIP propagation

For the semi-continuous propagation of PR8, a two-stage cultivation system was used, which consisted of two baffled shake flasks (250 mL baffled Erlenmeyer Flask, Thermo Fisher Scientific, 4116-0250) connected in series (Fig. 1B). The CSS and the VS were operated at a working volume of 90.00 mL and 77.52 mL, respectively. MDCK(sus) cells in exponential growth phase were seeded at a VCC of 0.6×10^6 cells/mL and were cultivated in batch mode at 185 rpm, and 37°C in a 5% CO_2 environment for 2 days. When VCC reached approximately 3.0×10^6 cells/mL, at -1.6 dpi, a calculated volume of cell suspension was harvested every 12 h, while pre-warmed fresh medium was added manually to obtain a RT (inverse of the dilution rate) of 38.3 h (both, CSS and VS). Please note that both shake flasks were not yet connected in series. After steady state was achieved, the cells in the VS were infected with PR8 at an MOI of 0.1 and trypsin (Thermo Fisher Scientific, #27250-018) was added (final activity of 20 U/mL). At 12 hpi, semi-continuous production was started by transferring cells from the CSS to the VS (V_2). Furthermore, virus was

harvested (V_4) and both shake flasks were filled up with pre-warmed fresh medium (V_1 or V_3) to obtain a RT of 38.3 h and 22.0 h for CSS and VS, respectively. Of importance is that the fresh medium, which was added to the VS, contained 60 U/mL trypsin to reach 20 U/mL in the VS. The respective transferred volumes are indicated (Equation 1–4). The RT of 22.0 h for the VS was chosen as previously published data showed a pronounced DIP/STV replication dynamic (31). In addition, samples were taken from the virus harvest at every volume transfer for analysis. Cell-free supernatants (300×g, 4°C, 5 min) were stored at -80°C for further analysis.

$$V_1 = (t_n - t_{n-1}) \cdot V_{CSS} \cdot D_{CSS} \quad (1)$$

$$V_2 = V_1 = (t_n - t_{n-1}) \cdot V_{CSS} \cdot D_{CSS} \quad (2)$$

$$V_3 = (t_n - t_{n-1}) \cdot (V_{VS} \cdot D_{VS} - V_{CSS} \cdot D_{CSS}) \quad (3)$$

$$V_4 = (t_n - t_{n-1}) \cdot D_{VS} \cdot V_{VS} \quad (4)$$

Where t_n denotes the sample time point, and t_{n-1} the previous sample time point. V_{CSS} is the volume of the CSS, V_{VS} is the volume of VS, D_{CSS} is the dilution rate of CSS, D_{VS} is the dilution rate of VS. V_{CSS}, D_{CSS}, D_{VS} were predefined as mentioned above. V_3 was set as $0.5 \times V_2$ to ensure a sufficient volume of fresh medium in the VS. This assumption was applied to calculate the volume of V_{Vs}.

4.3 Virus quantification

Quantification of the infectious virus titer was performed by $TCID_{50}$ assay as described previously (54) with a measurement error of ± 0.3 $\log_{10}$ (55). The active DIP titer (required for calculation of an MODIP for production of candidate DIPs in shake flasks, chapter 4.6.2) was quantified by plaque assay using MDCK-PB2(adh) cells (measurement error of ≤ 43.8%) (25). To determine the

512 infectious virus titers in the interference assay (chapter 4.7), MDCK(adh) cells were deployed in
513 the same plaque assay (25). In addition, an HA assay was used to quantify the total number of
514 virions in the supernatant with a measurement error of $\pm 0.15\ \log_{10}$(HAU/100 µL) (56).
515 Concentration of DIPs (c_{DIP}) or concentration of STVs (c_{STV}) were derived from the HA titer and
516 determined according to Equation 5, where c_{RBC} denotes the concentration of red blood cells
517 (2.0×10^7 cells/mL).

518 $$c_{DIP} = 10^{\frac{\log HA}{100\ \mu L}} \cdot c_{RBC} \qquad (5)$$

519 **4.4 PCR measurements**

520 Genomic vRNA in progeny virions were examined using PCR. In brief, isolation of vRNA from
521 150 µL cell-free supernatants was carried out with the NucleoSpin RNA virus kit (Macherey-
522 Nagel, 740956) as described in the manufacturers´ instructions. In order to analyze the presence of
523 FL vRNA and DI vRNA (truncated form), a segment-specific RT-PCR was performed (see 4.4.1).
524 Real-time RT-qPCR was applied for absolute quantification of Seg 5 vRNA from the progeny
525 virions (see 4.4.2).

526 **4.4.1 Segment-specific RT-PCR**

527 A recently described method was utilized for segment-specific RT-PCR (17, 30). In brief, isolated
528 vRNA was reverse transcribed into cDNA using universal primers that bind at the conserved
529 terminal regions of all eight IAV genome segments (Supplementary Table 1). Subsequently,
530 segment-specific primers were used for amplification of the respective genome segment sequence
531 by PCR (Supplementary Table 1). Finally, PCR products were analyzed by agarose gel
532 electrophoresis.

4.4.2 Real-time RT-qPCR

A recently reported method for the specific detection and quantification of influenza viral RNA segments using real-time RT-qPCR was employed (17, 57, 58). Briefly, RNA reference standards were *in vitro* synthesized for absolute quantification (primers required for generation are listed in Supplementary Table 4). Isolated vRNA of the samples was used for reverse transcription, along with a dilution series of the reference standards (primers listed in Supplementary Table 2), followed by real-time qPCR (primer sequence in Supplementary Table 3). Calculation for absolute quantification of vRNA of Seg 5 was conducted as previously described (17, 58).

4.4.3 NGS and data processing

Sample preparation, NGS library preparation and sequencing analysis of deletion junctions was performed according to a recently published study (32).

4.5 Analysis of deletion junctions

Deletion junctions refer to the DI vRNAs in the viral population, while deletion junction sites refer to the start and end position of the breaking points in the viral genome. Deletion junctions that did not accumulate to levels above 14 NGS reads in at least one sampling time point were removed from the data set for higher accuracy (32). Furthermore, defective vRNAs that showed more than 85 % of the length of FL vRNA were excluded from analysis in this work (except for Supplementary Fig. 3). DI vRNA 3´ and 5’ length indicated the number of retained nucleotides prior and after the deletion junction at the respective vRNA end. Of note is that DI vRNA sequence was reported in negative-sense and 3´ to 5´ orientation. The calculation of the DI vRNA length comprised the following sequence lengths: Seg 1 (2341 nucleotides (nt)), Seg 2 (2341 nt), Seg 3 (2233 nt), Seg 4 (1775 nt), Seg 5 (1565 nt), Seg 6 (1413 nt), Seg 7 (1027 nt), Seg 8 (890 nt).

555 Number of nucleotides of the incorporation signal (NCR) and the bundling signal (terminal ends
556 of coding region), which together form the packaging signal, were taken from a recent review (59).

557 **4.6 Generation of purely clonal DIPs containing a deletion in Seg 1**

558 To generate purely clonal Seg 1 derived DIPs (top gain, loss, gain (*de novo*)) in the absence of
559 STV, we used a previously established plasmid-based reverse-genetics system (41). More
560 specifically, to complement the missing PB2 to allow DIP production without STV, we used a co-
561 culture of HEK-293T-PB2 cells and MDCK-PB2(adh) cells for reconstitution.

562 **4.6.1 Generation of plasmids**

563 Plasmids harboring specific deletions were generated as described previously (41). In brief,
564 pHW191 encoding the PR8-derived PB2 gene (60) was used as a template for PCR amplification
565 (Phusion Hot Start II DNA polymerase, Thermo Fisher, #F549L). Here, the desired 5'-fragment
566 (containing overhangs complementary to the 3'-fragment) of a specified deletion junction
567 (Supplementary Table 5), using a 5'-specific forward and reverse primers set (Supplementary
568 Table 6) was used. Similarly, a set of 3'-specific primers were used to amplify the desired 3'-
569 fragment (containing overhangs complementary to the 5'-fragment) of a specified deletion junction
570 from the pHW191 template DNA. Next, the 5'-fragments hybridized with the overlapping 3´-
571 fragments, resulting in PCR products with the individual deletion junctions (splice-overlapped
572 products) after subsequent amplification cycles at an annealing temperature of 62°C. Lastly, the
573 internally spliced PB2 sequence was inserted in pHW2000-GGAarI using golden-gate cloning (61,
574 62). All plasmids were sequenced to confirm the generated deletion junctions.

4.6.2 Rescue and production of DIPs

For rescue of purely clonal DIPs containing a deletion in Seg 1 (41), we co-transfected a co-culture of adherent HEK-293T-PB2 cells (0.2×10^6 cells/well) and MDCK-PB2(adh) cells (0.2×10^6 cells/well) with corresponding plasmids harboring a deletion in the PB2 sequence (50 ng) and 1 µg of each pHW192-pHW198 plasmid (encoding for the remaining gene segments of PR8 IAV) using the calcium phosphate method in a 6-well format. DIP-containing supernatants were harvested at 4, 6, 8, 10, and 12 days post transfection and stored at -80°C for further use. Larger stocks (seed viruses) of purely clonal Seg 1 DIPs were generated in MDCK-PB2(sus) cells in shake flasks.

The production of Seg 1 DIPs in MDCK-PB2(sus) cells was conducted according to a recently published paper (25). In brief, MDCK-PB2(sus) cells, cultivated in shake flasks were centrifuged (300×g, 5 min, room temperature) and used to inoculate a new shake flask at 2.0×10^6 cells/mL with fresh media and trypsin (final activity of 20 U/mL). Subsequently, cells were infected at an MODIP of E-2. Cell-free supernatants (3000×g, 4°C, 10 min) were stored at -80°C for further analysis.

4.7 Interference assay

To measure the efficacy of DIPs to suppress STV replication, we performed an *in vitro* co-infection assay in MDCK(adh) cells following a previously published description (26). To summarize, MDCK(adh) cells, cultivated in 6-well plates, were washed twice with phosphate-buffered saline (PBS). Next, cells were either infected with STV only (MOI 0.01, based on the $TCID_{50}$ titer) or co-infected with STV and 125 µL of the produced DIP material (diluted for normalization, Supplementary Table 7). Wells were filled up to 250 µL with infection medium (GMEM, 1%

peptone, 5 U/mL trypsin) and incubation was conducted for 1 h at 37°C and 5% CO_2. Subsequently, the inoculum was aspirated, the cells washed with PBS and 2 mL of infection medium was added. Cells were incubated for 24 h at 37°C and 5% CO_2. The supernatant was harvested and stored at -80°C until further analysis by plaque assay and HA assay.

4.8 Data availability

The reference sequence of the PR8 genome used for alignment can be found under the following NCBI accession numbers: PB2 = AF389115.1, PB1 = AF389116.1, PA = AF389117.1, HA = AF389118.1, NP = AF389119.1, NA = AF389120.1, M = AF389121.1, NS = AF389122.1. The complete NGS dataset is available under the BioProject accession number PRJNA743179.

5 Conflict of Interest

A patent for the use of OP7 (a DIP containing point mutations instead of a deletion in Seg 7) as an antiviral agent for treatment of IAV infection is pending. Patent holders are S.Y.K. and U.R. Another patent for the use of DI244 and OP7 as an antiviral agent for treatment of coronavirus infection is pending. Patent holders are S.Y.K., U.R.

6 Author Contributions

Conceptualization, L.P., D.R., T.D., Y.G., C.B.B., S.Y.K. and U.R.; Formal analysis, L.P., D.R., F.G.A and S.Y.K.; Funding acquisition, C.B.B. and U.R; Investigation, L.P., D.R., T.D. and F.G.A.; Project administration, L.P. and S.Y.K.; Supervision, Y.G., C.B.B., S.Y.K. and U.R.; Visualization, L.P., D.R. and S.Y.K.; Writing – original draft, L.P., T.D. and S.Y.K.; Writing – review & editing, L.P., D.R., T.D., F.G.A., Y.G., C.B.B., S.Y.K. and U.R..

7 Acknowledgments

Special thanks to Claudia Best and Nancy Wynserski for their outstanding technical support. We thank Thomas Bissinger for providing the seed virus and Marc Hein for valuable discussions. The authors appreciate the sequencing work of Alvaro Hernandez, Christy Wright and the staff at the Roy. J. Carver Biotechnology Center, University of Illinois. We would like to thank St. Jude children research hospital, Memphis, United States for providing pHW2000 plasmids. Furthermore, a special thank is directed to Prof. Stefan Pöhlmann, Prerna Arora, and Najat Bdeir of the German Primate Center, Göttingen, Germany for providing plasmids and cell lines for rescue of DIP candidates and helpful discussions. We thank Shanghai BioEngine Sci-Tech and Prof. Tan from the East China University of Science and Technology for supplying the Xeno™ medium. The work was supported by the Defense Advanced Research Projects Agency (https://www.darpa.mil/program/intercept), INTERCEPT program under Cooperative Agreement W911NF-17-2-0012 and DARPA-16-35-INTERCEPT-FP-018.

8 References

1. Paget J, Spreeuwenberg P, Charu V, Taylor RJ, Iuliano AD, Bresee J, Simonsen L, Viboud C, Global Seasonal Influenza-associated Mortality Collaborator N, Teams* GLC. 2019. Global mortality associated with seasonal influenza epidemics: New burden estimates and predictors from the GLaMOR Project. J Glob Health 9:020421.
2. Taubenberger JK, Morens DM. 2020. The 1918 Influenza Pandemic and Its Legacy. Cold Spring Harb Perspect Med 10.
3. Moa AM, Chughtai AA, Muscatello DJ, Turner RM, MacIntyre CR. 2016. Immunogenicity and safety of inactivated quadrivalent influenza vaccine in adults: A systematic review and meta-analysis of randomised controlled trials. Vaccine 34:4092-4102.
4. Samson SI, Leventhal PS, Salamand C, Meng Y, Seet BT, Landolfi V, Greenberg D, Hollingsworth R. 2019. Immunogenicity of high-dose trivalent inactivated influenza vaccine: a systematic review and meta-analysis. Expert Rev Vaccines 18:295-308.
5. Vogel OA, Manicassamy B. 2020. Broadly Protective Strategies Against Influenza Viruses: Universal Vaccines and Therapeutics. Front Microbiol 11:135.

6. Tricco AC, Chit A, Soobiah C, Hallett D, Meier G, Chen MH, Tashkandi M, Bauch CT, Loeb M. 2013. Comparing influenza vaccine efficacy against mismatched and matched strains: a systematic review and meta-analysis. BMC Med 11:153.

7. Paules C, Subbarao K. 2017. Influenza. The Lancet 390:697-708.

8. O'Hanlon R, Shaw ML. 2019. Baloxavir marboxil: the new influenza drug on the market. Curr Opin Virol 35:14-18.

9. Hurt AC, Ernest J, Deng YM, Iannello P, Besselaar TG, Birch C, Buchy P, Chittaganpitch M, Chiu SC, Dwyer D, Guigon A, Harrower B, Kei IP, Kok T, Lin C, McPhie K, Mohd A, Olveda R, Panayotou T, Rawlinson W, Scott L, Smith D, D'Souza H, Komadina N, Shaw R, Kelso A, Barr IG. 2009. Emergence and spread of oseltamivir-resistant A(H1N1) influenza viruses in Oceania, South East Asia and South Africa. Antiviral Res 83:90-3.

10. Hayden FG, Sugaya N, Hirotsu N, Lee N, de Jong MD, Hurt AC, Ishida T, Sekino H, Yamada K, Portsmouth S, Kawaguchi K, Shishido T, Arai M, Tsuchiya K, Uehara T, Watanabe A, Baloxavir Marboxil Investigators G. 2018. Baloxavir Marboxil for Uncomplicated Influenza in Adults and Adolescents. N Engl J Med 379:913-923.

11. Jones JC, Kumar G, Barman S, Najera I, White SW, Webby RJ, Govorkova EA. 2018. Identification of the I38T PA Substitution as a Resistance Marker for Next-Generation Influenza Virus Endonuclease Inhibitors. mBio 9.

12. Dimmock NJ, Easton AJ. 2014. Defective interfering influenza virus RNAs: time to reevaluate their clinical potential as broad-spectrum antivirals? J Virol 88:5217-27.

13. Huo C, Cheng J, Xiao J, Chen M, Zou S, Tian H, Wang M, Sun L, Hao Z, Hu Y. 2020. Defective Viral Particles Produced in Mast Cells Can Effectively Fight Against Lethal Influenza A Virus. Front Microbiol 11:553274.

14. Zhao H, To KKW, Chu H, Ding Q, Zhao X, Li C, Shuai H, Yuan S, Zhou J, Kok KH, Jiang S, Yuen KY. 2018. Dual-functional peptide with defective interfering genes effectively protects mice against avian and seasonal influenza. Nat Commun 9:2358.

15. Yang Y, Lyu T, Zhou R, He X, Ye K, Xie Q, Zhu L, Chen T, Shen C, Wu Q, Zhang B, Zhao W. 2019. The Antiviral and Antitumor Effects of Defective Interfering Particles/Genomes and Their Mechanisms. Front Microbiol 10:1852.

16. Vignuzzi M, Lopez CB. 2019. Defective viral genomes are key drivers of the virus-host interaction. Nat Microbiol 4:1075-1087.

17. Kupke SY, Riedel D, Frensing T, Zmora P, Reichl U. 2019. A Novel Type of Influenza A Virus-Derived Defective Interfering Particle with Nucleotide Substitutions in Its Genome. J Virol 93:e01786-18.

18. Laske T, Heldt FS, Hoffmann H, Frensing T, Reichl U. 2016. Modeling the intracellular replication of influenza A virus in the presence of defective interfering RNAs. Virus Res 213:90-99.

19. Marriott AC, Dimmock NJ. 2010. Defective interfering viruses and their potential as antiviral agents. Rev Med Virol 20:51-62.

20. Nayak DP, Chambers TM, Akkina RK. 1985. Defective-Interfering (DI) RNAs of Influenza Viruses: Origin, Structure, Expression, and Interference, p 103-151. *In* Cooper M, Eisen H, Goebel W, Hofschneider PH, Koprowski H, Melchers F, Oldstone M, Rott R, Schweiger

HG, Vogt PK, Wilson I (ed), Current Topics in Microbiology and Immunology doi:10.1007/978-3-642-70227-3_3. Springer Berlin Heidelberg, Berlin, Heidelberg.

21. Duhaut SD, McCauley JW. 1996. Defective RNAs inhibit the assembly of influenza virus genome segments in a segment-specific manner. Virology 216:326-37.

22. Odagiri T, Tashiro M. 1997. Segment-specific noncoding sequences of the influenza virus genome RNA are involved in the specific competition between defective interfering RNA and its progenitor RNA segment at the virion assembly step. J Virol 71:2138-45.

23. Dimmock NJ, Dove BK, Meng B, Scott PD, Taylor I, Cheung L, Hallis B, Marriott AC, Carroll MW, Easton AJ. 2012. Comparison of the protection of ferrets against pandemic 2009 influenza A virus (H1N1) by 244 DI influenza virus and oseltamivir. Antiviral Res 96:376-85.

24. Dimmock NJ, Rainsford EW, Scott PD, Marriott AC. 2008. Influenza virus protecting RNA: an effective prophylactic and therapeutic antiviral. J Virol 82:8570-8.

25. Hein MD, Arora P, Marichal-Gallardo P, Winkler M, Genzel Y, Pohlmann S, Schughart K, Kupke SY, Reichl U. 2021. Cell culture-based production and in vivo characterization of purely clonal defective interfering influenza virus particles. BMC Biol 19:91.

26. Hein MD, Kollmus H, Marichal-Gallardo P, Puttker S, Benndorf D, Genzel Y, Schughart K, Kupke SY, Reichl U. 2021. OP7, a novel influenza A virus defective interfering particle: production, purification, and animal experiments demonstrating antiviral potential. Appl Microbiol Biotechnol 105:129-146.

27. Easton AJ, Scott PD, Edworthy NL, Meng B, Marriott AC, Dimmock NJ. 2011. A novel broad-spectrum treatment for respiratory virus infections: influenza-based defective interfering virus provides protection against pneumovirus infection in vivo. Vaccine 29:2777-84.

28. Scott PD, Meng B, Marriott AC, Easton AJ, Dimmock NJ. 2011. Defective interfering influenza A virus protects in vivo against disease caused by a heterologous influenza B virus. J Gen Virol 92:2122-2132.

29. Rand U, Kupke SY, Shkarlet H, Hein MD, Hirsch T, Marichal-Gallardo P, Cicin-Sain L, Reichl U, Bruder D. 2021. Antiviral Activity of Influenza A Virus Defective Interfering Particles against SARS-CoV-2 Replication In Vitro through Stimulation of Innate Immunity. Cells 10.

30. Frensing T, Heldt FS, Pflugmacher A, Behrendt I, Jordan I, Flockerzi D, Genzel Y, Reichl U. 2013. Continuous influenza virus production in cell culture shows a periodic accumulation of defective interfering particles. PLoS One 8:e72288.

31. Tapia F, Laske T, Wasik MA, Rammhold M, Genzel Y, Reichl U. 2019. Production of Defective Interfering Particles of Influenza A Virus in Parallel Continuous Cultures at Two Residence Times-Insights From qPCR Measurements and Viral Dynamics Modeling. Front Bioeng Biotechnol 7:275.

32. Alnaji FG, Holmes JR, Rendon G, Vera JC, Fields CJ, Martin BE, Brooke CB. 2019. Sequencing Framework for the Sensitive Detection and Precise Mapping of Defective Interfering Particle-Associated Deletions across Influenza A and B Viruses. J Virol 93.

730 33. Davis AR, Nayak DP. 1979. Sequence relationships among defective interfering influenza
731 viral RNAs. Proc Natl Acad Sci U S A 76:3092-6.

732 34. Duhaut SD, Dimmock NJ. 1998. Heterologous protection of mice from a lethal human
733 H1N1 influenza A virus infection by H3N8 equine defective interfering virus: comparison
734 of defective RNA sequences isolated from the DI inoculum and mouse lung. Virology
735 248:241-53.

736 35. Jennings PA, Finch JT, Winter G, Robertson JS. 1983. Does the higher order structure of
737 the influenza virus ribonucleoprotein guide sequence rearrangements in influenza viral
738 RNA? Cell 34:619-627.

739 36. Saira K, Lin X, DePasse JV, Halpin R, Twaddle A, Stockwell T, Angus B, Cozzi-Lepri A,
740 Delfino M, Dugan V, Dwyer DE, Freiberg M, Horban A, Losso M, Lynfield R, Wentworth
741 DN, Holmes EC, Davey R, Wentworth DE, Ghedin E, Group IFS, Group IFS. 2013.
742 Sequence analysis of in vivo defective interfering-like RNA of influenza A H1N1 pandemic
743 virus. J Virol 87:8064-74.

744 37. Tapia F, Jordan I, Genzel Y, Reichl U. 2017. Efficient and stable production of Modified
745 Vaccinia Ankara virus in two-stage semi-continuous and in continuous stirred tank
746 cultivation systems. PLoS One 12:e0182553.

747 38. Routh A, Johnson JE. 2014. Discovery of functional genomic motifs in viruses with
748 ViReMa-a Virus Recombination Mapper-for analysis of next-generation sequencing data.
749 Nucleic Acids Res 42:e11.

750 39. Fujii Y, Goto H, Watanabe T, Yoshida T, Kawaoka Y. 2003. Selective incorporation of
751 influenza virus RNA segments into virions. Proc Natl Acad Sci U S A 100:2002-7.

752 40. Goto H, Muramoto Y, Noda T, Kawaoka Y. 2013. The genome-packaging signal of the
753 influenza A virus genome comprises a genome incorporation signal and a genome-bundling
754 signal. J Virol 87:11316-22.

755 41. Bdeir N, Arora P, Gartner S, Hoffmann M, Reichl U, Pohlmann S, Winkler M. 2019. A
756 system for production of defective interfering particles in the absence of infectious
757 influenza A virus. PLoS One 14:e0212757.

758 42. Widjaja I, de Vries E, Rottier PJ, de Haan CA. 2012. Competition between influenza A
759 virus genome segments. PLoS One 7:e47529.

760 43. Hutchinson EC, von Kirchbach JC, Gog JR, Digard P. 2010. Genome packaging in
761 influenza A virus. J Gen Virol 91:313-28.

762 44. Noda T, Kawaoka Y. 2010. Structure of influenza virus ribonucleoprotein complexes and
763 their packaging into virions. Rev Med Virol 20:380-91.

764 45. Duhaut S, Dimmock NJ. 2000. Approximately 150 nucleotides from the 5' end of an
765 influenza A segment 1 defective virion RNA are needed for genome stability during
766 passage of defective virus in infected cells. Virology 275:278-85.

767 46. Duhaut SD, Dimmock NJ. 2002. Defective segment 1 RNAs that interfere with production
768 of infectious influenza A virus require at least 150 nucleotides of 5' sequence: evidence
769 from a plasmid-driven system. J Gen Virol 83:403-411.

770 47. Ueda M, Nakajima K, Sugiura A. 1980. Extra RNAs of von Magnus particles of influenza
771 virus cause reduction of particular polymerase genes. J Virol 34:1-8.

48. Alnaji FG, Reiser WK, Velthuis At, Brooke CB. 2021. Influenza A virus defective viral genomes are inefficiently packaged into virions relative to wild-type genomic RNAs. bioRxiv doi:10.1101/2021.05.13.444068:2021.05.13.444068.

49. Levi LI, Rezelj VV, Henrion-Lacritick A, Erazo D, Boussier J, Vallet T, Bernhauerova V, Suzuki Y, Carrau L, Weger-Lucarelli J, Saleh MC, Vignuzzi M. 2021. Defective viral genomes from chikungunya virus are broad-spectrum antivirals and prevent virus dissemination in mosquitoes. PLoS Pathog 17:e1009110.

50. Rezelj VV, Carrau L, Merwaiss F, Levi LI, Erazo D, Tran QD, Henrion-Lacritick A, Gausson V, Suzuki Y, Shengjuler D, Meyer B, Vallet T, Weger-Lucarelli J, Bernhauerova V, Titievsky A, Sharov V, Pietropaoli S, Diaz-Salinas MA, Legros V, Pardigon N, Barba-Spaeth G, Brodsky L, Saleh MC, Vignuzzi M. 2021. Defective viral genomes as therapeutic interfering particles against flavivirus infection in mammalian and mosquito hosts. Nat Commun 12:2290.

51. Welch SR, Tilston NL, Lo MK, Whitmer SLM, Harmon JR, Scholte FEM, Spengler JR, Duprex WP, Nichol ST, Spiropoulou CF. 2020. Inhibition of Nipah Virus by Defective Interfering Particles. J Infect Dis 221:S460-S470.

52. Lohr V, Genzel Y, Behrendt I, Scharfenberg K, Reichl U. 2010. A new MDCK suspension line cultivated in a fully defined medium in stirred-tank and wave bioreactor. Vaccine 28:6256-64.

53. Bissinger T, Fritsch J, Mihut A, Wu Y, Liu X, Genzel Y, Tan WS, Reichl U. 2019. Semi-perfusion cultures of suspension MDCK cells enable high cell concentrations and efficient influenza A virus production. Vaccine 37:7003-7010.

54. Genzel Y, Reichl U. 2007. Vaccine Production, p 457-473. *In* Pörtner R (ed), Animal Cell Biotechnology doi:10.1007/978-1-59745-399-8_21. Humana Press, Totowa, NJ.

55. Genzel Y, Rödig J, Rapp E, Reichl U. 2014. Vaccine Production: Upstream Processing with Adherent or Suspension Cell Lines, p 371-393. *In* Pörtner R (ed), Animal Cell Biotechnology: Methods and Protocols doi:10.1007/978-1-62703-733-4_23. Humana Press, Totowa, NJ.

56. Kalbfuss B, Knochlein A, Krober T, Reichl U. 2008. Monitoring influenza virus content in vaccine production: precise assays for the quantitation of hemagglutination and neuraminidase activity. Biologicals 36:145-61.

57. Kawakami E, Watanabe T, Fujii K, Goto H, Watanabe S, Noda T, Kawaoka Y. 2011. Strand-specific real-time RT-PCR for distinguishing influenza vRNA, cRNA, and mRNA. J Virol Methods 173:1-6.

58. Frensing T, Kupke SY, Bachmann M, Fritzsche S, Gallo-Ramirez LE, Reichl U. 2016. Influenza virus intracellular replication dynamics, release kinetics, and particle morphology during propagation in MDCK cells. Appl Microbiol Biotechnol 100:7181-92.

59. Breen M, Nogales A, Baker SF, Martinez-Sobrido L. 2016. Replication-Competent Influenza A Viruses Expressing Reporter Genes. Viruses 8.

60. Hoffmann E, Neumann G, Kawaoka Y, Hobom G, Webster RG. 2000. A DNA transfection system for generation of influenza A virus from eight plasmids. Proc Natl Acad Sci U S A 97:6108-13.

814 61. Andreou AI, Nakayama N. 2018. Mobius Assembly: A versatile Golden-Gate framework
815 towards universal DNA assembly. PLoS One 13:e0189892.

816 62. Engler C, Gruetzner R, Kandzia R, Marillonnet S. 2009. Golden gate shuffling: a one-pot
817 DNA shuffling method based on type IIs restriction enzymes. PLoS One 4:e5553.

818